RSC Advances

PAPER

View Article Online
View Journal | View Issue

Cite this: *RSC Adv.*, 2020, **10**, 7289

Sustained delivery of PlGF-$2_{123\text{-}144*}$-fused BMP2-related peptide P28 from small intestinal submucosa/polylactic acid scaffold material for bone tissue regeneration

Zekang Xiong, †[a] Wei Cui,†[b] Tingfang Sun,†[a] Yu Teng,[c] Yanzhen Qu,[a] Liang Yang,[a] Jinge Zhou,[a] Kaifang Chen,[a] Sheng Yao,[a] Zengwu Shao[a] and Xiaodong Guo*[a]

Received 27th September 2019
Accepted 9th February 2020

DOI: 10.1039/c9ra07868a

rsc.li/rsc-advances

Bone morphogenetic protein 2 (BMP-2) is one of the most important factors for bone tissue formation. However, its use over the past decade has been associated with numerous side effects. This is due to the fact that recombinant human (rh) BMP-2 has several biological functions, as well as that non-physiological high dosages were commonly administered. In this study, we synthesized a novel BMP-2-related peptide (designated P28) and fused a mutant domain in placenta growth factor-2 (PlGF-$2_{123\text{-}144*}$) that allowed for the "super-affinity" of extracellular matrix proteins to P28, effectively controlling the release of low dosage P28 from small intestinal submucosa/polylactic acid (SIS/PLA) scaffolds. These have been shown to be excellent scaffold materials both *in vivo* and *in vitro*. The aim of this study was to determine whether these scaffolds could support the controlled release of P28 over time, and whether the composite materials could serve as structurally and functionally superior bone substitutes *in vivo*. Our results demonstrated that P28 could be released slowly from SIS/PLA to promote the adhesion, proliferation, and differentiation of bone marrow stromal cells (BMSCs) *in vitro*. *In vivo*, radiographic and histological examination showed that SIS/PLA/P28/PlGF-$2_{123\text{-}144*}$ completely repaired critical-size bone defects, compared to SIS/PLA, SIS/PLA/PlGF-$2_{123\text{-}144*}$, or SIS/PLA/P28 alone. These findings suggest that this controlled release system may have promising clinical applications in bone tissue engineering.

1. Introduction

Several millions of patients worldwide suffer from bone defects due to trauma, cancer, and bone disease, most of whom exhibit a wide range of defects that are difficult to treat and are problematic for clinical orthopaedics.[1] The success rate for autologous bone grafts can be as high as 80–90%; these therefore are considered the "gold standard" for bone defect repair.[2,3] However, their application is restricted due to limited sources of donor material, new defects at the donor site, and the extended duration of surgery.[4–6] Artificial bone materials can make up for the lack of autologous bone to some extent,[7] however the host immune response and the potential risk of implant rejection and infectious diseases pose a challenge in overcoming their shortcomings.[8,9] Therefore, the development of a more efficient bone repair material is a primary goal for researchers in this field.[10–14]

Recently, natural extracellular matrix (ECM) derived from small intestinal submucosa (SIS) has drawn increasing attention due to its superior bioactivity and biomimetic microenvironment in osteogenic differentiation and bone remodeling.[15,16] The main components of decellularized SIS are collagen I and glycosaminoglycans, which contain multifarious bioactive proteins, including fibronectin, tenascin C, fibrinogen, and growth factors. Meanwhile, SIS has non-immunogenic characteristic, including its avoidance of excessive immune response and implantation rejection *in vivo*.[17] Considering the many merits of SIS, it is possible for modified SIS materials to replace other artificial bone materials as a new natural composite material for repairing segmental bone defects.

Bone morphogenetic proteins (BMPs) are members of the transforming growth factor-β superfamily (TGF-β) and have been shown to exhibit the strongest bone induction activity among bone growth factors.[18] However, large, non-physiological doses of rhBMP-2 have been customarily used because of its short half-life *in vivo*. This has led to the occurrence of

[a]*Department of Orthopedics, Union Hospital, Tongji Medical College, Huazhong University of Science and Technology, 1277 Jiefang Avenue, Wuhan 430022, People's Republic of China. E-mail: Xiaodongguo@hust.edu.cn; Tel: +86 15327216660*

[b]*Department of Orthopedics, Wuhan Fourth Hospital, Puai Hospital, Tongji Medical College, Huazhong University of Science and Technology, Wuhan, 430000, People's Republic of China*

[c]*Department of Orthopedics, Central Hospital of Wuhan, Tongji Medical College, Huazhong University of Science and Technology, Wuhan 430014, People's Republic of China*

† Zekang Xiong, Wei Cui, and Tingfang Sun contributed equally to this work.

numerous side effects, such as inflammatory reactions, radiculitis, urinary retention, bone resorption, and cancer risk.[19–23] To surmount the shortcomings of rhBMP-2, we designed a novel BMP2-mimicking peptide (P28, MW: 3091.20) according to the residues of the knuckle epitope of BMP-2. The P28 peptide was confirmed to display effects of bone formation similar to those of BMP-2 in a rat model.[24–26] In addition, the short block of seven repeated aspartic acid, linked to phosphorylated serine motifs, have a higher affinity to hydroxyapatite. In general, the growth factor would significantly increase the rate of release and degradation *in vivo*, which are the key limiting factors in the translation of growth factors to clinical use in regenerative medicine.

A recent study identified a domain of placental growth factor 2 (PlGF-$2_{123\text{-}144}$) with "super-affinity" to ECM protein (collagen I, fibronectin, *etc.*). *In vivo*, PlGF-$2_{123\text{-}144}$-fused BMP-2 was strongly retained in a fibrin matrix and facilitated a prominent increase of bone tissue deposition in a cranial defect zone.[27] These findings provide a basis from which improve the limited efficacy and rapid degradation of growth factors in bone defect preclinical models. Nevertheless, PlGF-$2_{123\text{-}144}$-fused growth factors have not yet been demonstrated to accelerate endochondral ossification other than endochondral ossification administered on the dura in cranial defect models.

Considering this intrinsic property of PlGF-$2_{123\text{-}144}$, it is of great interest to determine whether the new structural grafted protein (P28/PlGF-$2_{123\text{-}144}$) is endowed with an enhanced affinity to ECM. SIS/PLA was chosen to be the scaffold for the content of proteins containing binding sites, which have a high-affinity to PlGF-2. PLA is often used as a biodegradable polymer in bone fixation systems. PLA reinforce composites because of its superior mechanical performance for segmental bone defects.[28] In this study, we hypothesized that the new biomimetic composite impregnating P28/PlGF-$2_{123\text{-}144}$ into SIS/PLA scaffold will provide a better microenvironment for BMSC adhesion, proliferation, and osteodifferentiation. SIS/PLA composite materials could control the release of P28/PlGF-$2_{123\text{-}144}$ over time *in vitro* and could serve as a functionally superior bone substitute material *in vivo* for potential applications in clinical settings in the treatment of massive bone defects.

2. Materials and methods

2.1. Synthesis of P28 and P28/PlGF-$2_{123\text{-}144}$*

As the steric effect of cysteine impaired the production of the fusion protein, we synthesized a version of PlGF-$2_{123\text{-}144}$ where cysteine-142 was substituted by serine (PlGF-$2_{123\text{-}144}$*), followed by its fusion to the C-terminus of BMP-2-derived peptide P28 to obtain P28/PlGF-$2_{123\text{-}144}$*. The P28 and P28/PlGF-$2_{123\text{-}144}$* were synthesized using Fmoc/*t*Bu solid-phase peptide synthesis. The crude peptide chemistry produced from this synthesis method was subjected to preliminary purification by gel filtration, followed by high performance liquid chromatography (HPLC) to obtain PlGF-$2_{123\text{-}144}$*, P28, and P28/PlGF-$2_{123\text{-}144}$* with purities of 97.38%, 96.13%, and 96.29%, respectively. The protein sequences are shown in Table 1.

2.2. Preparation of SIS/PLA

SIS powder was synthesized as previously described.[29] Briefly, porcine jejunum was harvested from healthy home raised pigs (around 100 kg at 6 months) within 3 h of sacrifice. This was sequentially subjected to mechanical dissociation, degreasing, enzyme digestion, detergent, lyophilization, and sterilization into 10–20 mm powder. To prepare the SIS/PLA scaffolds, the SIS powder was added to 5%, 8% PLA solution (dissolved in dioxane (m/v)) at a 1 : 1 SIS : PLA weight ratio. The solution was ultrasonicated, poured into a cubical/circular/cylindrical polymethyl methacrylate mold, frozen at −80 °C overnight, and then lyophilized to remove dioxane. Hereafter, SIS/8% PLA is simply referred to as SIS/PLA as it was the primary composite scaffold under investigation.

2.3. Preparation of composite materials

The SIS/PLA scaffolds (Fig. 1d) were shaped into three types of specifications: small cubes (5 mm × 5 mm × 5 mm), circular slices (Φ10 mm × 2 mm), and cylinders (Φ10 mm × 20 mm). The PlGF-$2_{123\text{-}144}$*, P28, and P28/PlGF-$2_{123\text{-}144}$* proteins were dissolved in deionized water to generate 2 and 5 mg mL^{-1} concentrations. The small cube and circular slice materials were soaked in 1 mL protein solution (2 mg mL^{-1}) and the large cylinder materials were soaked in 4 mL protein solution (5 mg mL^{-1}). These mixtures of material and solution were placed at −20 °C overnight, and then placed in a vacuum drying oven for vacuum aspiration for 24 h before freezing at −55 °C for 48 h. Finally, all materials were disinfected by ethanol evaporation and stored at −20 °C until further use.

2.4. Scaffold characterization

The microstructure of the SIS, SIS/5% PLA, and SIS/8% PLA scaffolds were characterized by scanning electron microscope (SEM). Small pieces with a razor blade of vacuum dried scaffolds were observed after being sputter coated with a layer of platinum, approximately 10 nm thick, and further processed using NIH ImageJ software.

The porosity of the scaffolds was measured according to Archimedes' principle.[30] Three samples (Φ10 mm × 20 mm) for each group were used for the measurement and water was used as liquid medium. The porosity (P) was calculated using the following formula: $P = (W_2 - W_1)/(W_2 - W_3) \times 100\%$, where W_1 is the dry weight of the scaffold, W_2 is the weight of the scaffold saturated with water, and W_3 is the weight of the scaffold suspended in water. The mechanical properties of the SIS, SIS/5% PLA, and SIS/8% PLA cylinders (Φ20 mm × 10 mm) were evaluated as previously described.[31] Five specimens of each group were used for compressive mechanical test and compressive strength using a computer-controlled universal testing machine (ElectroPuls E1000; Instron, Inc.) at a crosshead speed of 0.5 mm min^{-1}.

Table 1 Protein sequences of PlGF-$2_{123\text{-}144}$, PlGF-$2_{123\text{-}144*}$, P28, and P28/PlGF-$2_{123\text{-}144*}$

PlGF-$2_{123\text{-}144}$	RRRPKGRGKRRREKQRPTDCHL
PlGF-$2_{123\text{-}144*}$	RRRPKGRGKRRREKQRPTDSHL
P28	$S^{[PO4]}$ DDDDDDDKIPKASSVPTELSAISTLYL
P28/PlGF-$2_{123\text{-}144*}$	$S^{[PO4]}$ DDDDDDDKIPKASSVPTELSAISTLYLRRRPKGRGKRRREKQRPTDSHL

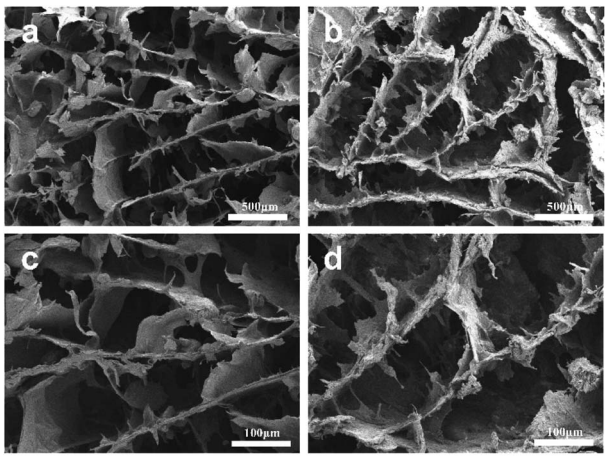

Fig. 1 SEM micrographs of SIS/5% PLA and SIS/8% PLA at various magnifications: 50× (a and b) and 100× (c and d).

2.5. FITC-P28, FITC-PlGF-$2_{123\text{-}144*}$, and FITC-P28/PlGF-$2_{123\text{-}144*}$ coating efficiency assay

To compare the affinity of P28, PlGF-$2_{123\text{-}144*}$, and P28/PlGF-$2_{123\text{-}144*}$ to the SIS/PLA scaffold, 1 mL of FITC-peptide at a final concentration of 0.1 mM was added to the circular slices scaffold dissolved in 1× phosphate buffered solution (PBS), as previously described.[32] The SIS/PLA was then incubated for 1 h with gentle rotation at −20 °C, followed by washing three times with 1 mL of 1× PBS to remove any unbound FITC-peptide. The optical density of the bound FITC-peptide was quantified by measuring the amount of FITC remaining in the PBS solution at a wavelength of 490 nm using a multi-detection microscope reader (BioTek Instruments).

2.6. Enzymatic release of P28 peptide from SIS/PLA

The SIS/PLA/P28/PlGF-$2_{123\text{-}144*}$ scaffolds were transferred to 2 mL sterile PBS solution with or without 4 mg mL^{-1} of collagenase type I (Sigma-Aldrich) or 100 μU of plasmin (Roche) at 37 °C for 21 days. The SIS/PLA/P28 scaffolds placed in pure PBS solution served as a control group. The eluate of the P28 peptide was detected at 12 h and 1, 2, 3, 5, 7, 10, 12, 14, 18, and 21 days after incubation. The supernatant was completely removed and replaced with fresh enzymatic solution at each time interval. The amount of P28 peptide in the collected supernatant was detected by HPLC, as previously described.[33]

2.7. Bone marrow stromal cell culture

Bone marrow stromal cells (BMSCs) were purchased from the China Center for Type Culture Collection (Wuhan University). The BMSC media consisted of α-modified Eagle's medium (α-MEM) supplemented with 15% fetal bovine serum (FBS), 10 mM Na-β-glycerol phosphate (Sigma-Aldrich, St. Louis, MO, USA), 50 μg mL^{-1} ascorbic acid (Sigma-Aldrich), antibiotic-antimycotic solution, and 10^{-8} M dexamethasone. The cells were incubated under 95% air and 5% CO_2 at 37 °C. When the cells reached 80% confluence, they were detached using 0.25% trypsin-1 mM EDTA-4Na and seeded in two new cell culture bottles to continue incubation; this was repeated until the cells were cultured to the third generation.

2.8. Evaluation of cell viability and proliferation

Calcein-AM/propidium iodide double staining (live/dead assay; Sigma-Aldrich) was used to quantify cell viability. The cell adhesion rates were measured 24 h after BMSCs (third generation, 5×10^5 per well) and been seeded onto the SIS/5% PLA and SIS/8% PLA scaffolds. The BMSCs were then cultured with the four biomaterials, namely SIS/PLA, SIS/PLA, SIS/PLA/PlGF-$2_{123\text{-}144*}$, SIS/PLA/P28, and SIS/PLA/P28/PlGF-$2_{123\text{-}144*}$ (small cubes), respectively, in 24-well plates, and incubated under 95% air and 5% CO_2 at 37 °C. After 7 days of culture, the attached cells from each sample were counted according to the manufacturer's protocol. The attached cells were visualized using a fluorescence microscopy (OLYMPUS, Japan). In order to quantify the number of live cells, 15 images for each time point from three specimens for each group using ImageJ software.

Cell proliferation was detected using the MTT assay (Beyotime Biotechnology, Shanghai, China), as described previously.[34] Briefly, the cell-seeded scaffold (circular slices) was washed and incubated in MTT solution for 3 h at 37 °C. The scaffold was then dissolved in dimethyl sulfoxide to dissolve the formazan crystals. Removing 100 μL per well extract into 96-well plate to measure its absorbance at 540 nm wavelength.

2.9. Alkaline phosphatase (ALP) staining and quantitative analyses

The BMSCs were seeded at a density of 5×10^5/scaffold onto the SIS/PLA, SIS/PLA/PlGF-$2_{123\text{-}144*}$, SIS/PLA/P28, and SIS/PLA/P28/PlGF-$2_{123\text{-}144*}$ (small cubes) scaffolds in 24-well plates, then incubated under 95% air and 5% CO_2 at 37 °C. After 24 h, the medium was exchanged with bone differentiation medium. The alkaline phosphatase (ALP) activity was measured using an ALP protein assay kit (Beyotime Biotechnology, Shanghai, China). After 5, 10, and 15 days, the cells were evaluated for alkaline phosphatase (ALP) activity at 520 nm.

2.10. Protein isolation and western blotting

After 7 days incubation on circular slices, all the total protein lysates were isolated using RIPA (Aspen, China) supplemented with phenylmethanesulfonyl fluoride, protease, and phosphatase inhibitors (Aspen, China). These were then sonicated on ice before determining the protein concentrations using a BCA protein assay kit (Sigma-Aldrich). The extracted proteins were resolved on 10% SDS-PAGE gels and blotted onto PVDF membranes (EMD Millipore Corporation, USA), which was blocked with 5% non-fat dry milk in TBST at room temperature for 1 h. The membranes were incubated with primary antibodies against anti-Col-1α (Proteintech), anti-Runx2 (Abcam), anti-OPN (Proteintech), anti-OCN (Abcam), anti-Smad1/5/8 (Abcam), anti-phospho-Smad1/5/8 (CST), anti-β-actin (Proteintech) overnight at 4 °C. After washing with TBST three times, the protein bands were developed by incubating the membranes with horseradish peroxidase (HRP)-conjugated secondary antibody at room temperature for 1 h, followed by detection using enhanced chemiluminescent detection reagents.

2.11. RNA extraction and qPCR

Total RNA was extracted using a RNeasy Mini Kit (Qiagen, Valencia, CA, USA), according to the manufacturer's protocols. The quantity of total RNA was measured by spectrophotometry. Complementary DNA was synthesized using a First Strand cDNA Synthesis Kit (TAKARA, Japan) according to the manufacturer's instructions. Real-time polymerase chain reaction (RT-PCR) was performed on a 96-well plate ABI Prism 7500 (Applied Biosystems, Foster City, CA) using a KAPA SYBR FAST qPCR Kit Master Mix. Relative expression was calculated using the $2^{-\Delta\Delta C_t}$ method normalized to β-actin.

2.12. Model of canine radial defects and surgical procedures

All animal procedures were performed in accordance with the Guidelines for Care and Use of Laboratory Animals of Huazhong University of Science and Technology (HUST, Wuhan, China) and approved by the Institutional Animal Care and Use Committee at Tongji Medical College, HUST. We purchased 9–11 kg male Beagle canines from the Animal Center of Tongji Medical College. The dogs were kept in separate cages, fed a standard diet, and allowed to remain mobile during the study. A total of 30 male Beagle canines were each subjected to a bilateral radial defect model, and randomly divided into five groups: control (no implant), SIS/PLA, SIS/PLA/PlGF-$2_{123\text{-}144*}$, SIS/PLA/P28, and SIS/PLA/P28/PlGF-$2_{123\text{-}144*}$. Each group contained 6 canines and the bilateral radius of each canine was made to model. After each dog was anaesthetized with an intramuscular injection of sumianxin (0.08 mL kg^{-1}) and an intraperitoneal injection of 3% sodium pentobarbital (0.5 mL kg^{-1}), surgery was performed under sterile conditions. The bilateral forelimbs were clipped and scrubbed with povidone-iodine and a 70% ethanol solution. Then, the radial medial surgical approach was utilized by separating the fascia and muscle, exposing the middle segment of both the radial and ulna. A 20 mm segmental defect was made in the radial using a burr drill with irrigation by sterile saline. Both ends of the defect were fixed with a steel plate after the materials associated with each group had been implanted into the defect. The soft tissue and skin were then closed by suturing (Fig. 1b). The Lane–Sandhu X-ray criteria were used to quantitatively evaluate the effects of the massive bone defect in the five groups.[26]

2.13. Radiographic examination

All canines were anaesthetized with an intramuscular injection of sumianxin (0.08 mL kg^{-1}) and intraperitoneal injection of 3% sodium pentobarbital (0.5 mL kg^{-1}) at 12 and 24 weeks after surgery. Once the canines were completely anaesthetized, their bilateral forelimbs were respectively radiographed by X-ray (DRX-Evolution, Carestream Health, Rochester, NY, USA). All of the canines were sacrificed at 24 weeks and the bones were cut out at the distal and proximal 5 mm from the defect area of the radial bone. The repair of the defect area was observed using 3-dimensional-computerised tomography (3D-CT) (Discovery CT750 HD, General Electric, Fairfield, CT, USA). Coverage was calculated on a dorsoventral projection of the cylindrical area.

2.14. Histological analysis

For histological examination, the samples were fixed in 10% neutral formalin and subsequently decalcified in 10% ethylenediaminetetraacetic acid (EDTA, pH 7.0). The samples were embedded in paraffin after being completely decalcified. Serial slices of 5 μm were then sectioned using a microtome, followed by staining with hematoxylin and eosin (H&E) and Masson for microscopic observation.

Immunohistochemical (IHC) staining was performed to detect the expression of osteocalcin (OCN), an osteogenic marker, as described previously.[16] The deparaffinized sections were first incubated in hydrogen peroxide for blocking endogenous peroxidase activity, followed by incubation with primary mouse monoclonal antibodies: anti-OCN (1 : 200 dilution) at 4 °C overnight. After washing thrice with PBS, the sections were incubated with secondary antibody (Proteintech) for 20 min, followed by buffered 3,3-diaminobenzidine tetrahydrochloride (DAB) as chromogen.

To compare the area of new bone formation and OCN-positive area among the images of histological sections, semi-quantitative analysis was performed on the H&E-stained histological sections and the immunohistochemical sections. Images of the sections were taken using an Olympus BX51 light microscope equipped with a change coupled device camera (Olympus, Tokyo, Japan). Two sections were chosen for each sample, which were observed under a microscope at 40× magnification. Then, 4 images were chosen randomly from within a single section. The images were analyzed using Image-Pro plus software (Media Cybernetics, Rockville, MD, USA).

2.15. Statistical analysis

All numerical data were expressed as means ± standard deviation (SD). ANOVA was used to test for statistical significance in GraphPad Prism 6 (GraphPad Software, La Jolla, CA, USA).

Tukey's *post hoc* test was used to compare individual pairs of groups. $p < 0.05$ was considered statistically significant.

3. Results

3.1. Scaffold characterization

The SIS/PLA material appeared as a white block (Fig. 7a). The slice layer pore structure is shown in Fig. 1. The SEM images of SIS/PLA show polygonal pores arranged in an irregular manner, with thick walls and a larger number of micro-pores, with an overall pore size of 100–300 μm. We designed SIS with PLA of two concentrations, SIS/5% PLA and SIS/8% PLA. SIS/5% PLA and SIS/8% PLA showed a similar pore size range. The density of normal spindle morphologic live BMSCs stained with calcein-AM (green) showed on significantly difference on all members at 24 h (Fig. 2a). PLA was found to markedly reinforce the biomechanical strength of the SIS scaffold. We compared the compressive strength (CS) and compressive modulus (CM) of pure SIS, SIS/5% PLA, and SIS/8% PLA. The CS value of SIS/8% PLA was 1.9 ± 0.49 MPa. No significant enhancement of the compressive property was observed for 8% PLA, despite a higher concentration of PLA than SIS/5% PLA (Fig. 2b). The CM value of SIS/8% PLA was 10.89 ± 1.60 MPa, nearly 34-fold higher than that of the SIS scaffold ($p < 0.05$). Moreover, the SIS/8% PLA scaffold had significantly higher compressive modulus than SIS/5% PLA scaffold (7.19 ± 1.89 MPa) (Fig. 2c).

3.2. FITC-P28, FITC-PlGF-$2_{123\text{-}144*}$, and FITC-P28/PlGF-$2_{123\text{-}144*}$ binding efficiency

The absorption of P28, PlGF-$2_{123\text{-}144*}$, and P28/PlGF-$2_{123\text{-}144*}$ to SIS/PLA was assessed by quantifying the FITC-labelled peptide bound to the SIS matrix proteins (collagen I, fibronectin, fibrinogen). As shown in Fig. 3, FITC-PlGF-$2_{123\text{-}144*}$ and FITC-P28/PlGF-$2_{123\text{-}144*}$ showed a significantly higher optical density value than FITC-P28, indicating a stronger affinity to the SIS/PLA scaffold.

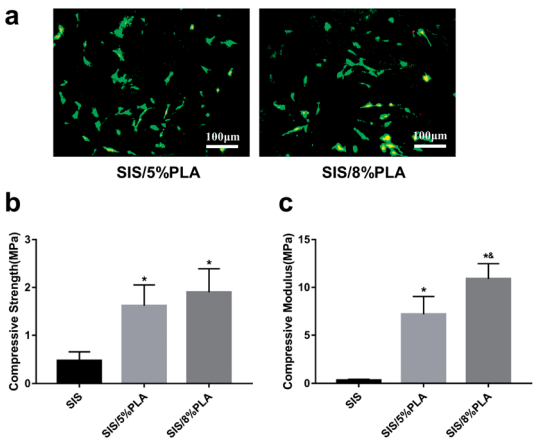

Fig. 2 (a) Representative fluorescence images of cells on SIS/5% PLA and SIS/8% PLA at 24 h. (b) The compressive strength (b) and compressive modulus (c) of SIS/5% PLA and SIS/8% PLA. Statistical significance is indicated by $*p < 0.05$ compared with the SIS group, and $^{\delta}p < 0.05$ compared with the SIS/5% PLA group. Error bars represent standard deviations from the mean ($n = 5$).

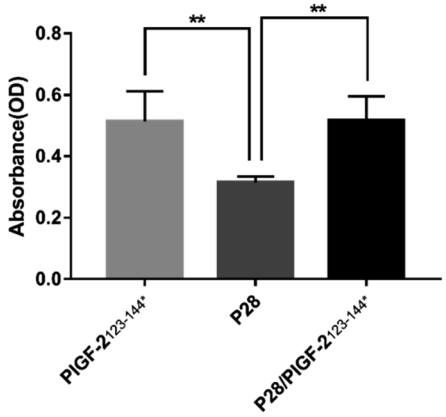

Fig. 3 FITC-P28, FITC-PlGF-$2_{123\text{-}144*}$, and FITC-P28/PlGF-$2_{123\text{-}144*}$ bound to the SIS/PLA scaffold. Peptide coating solutions were detected for depletion of fluorescence and the percentage of peptide bound to scaffold was calculated ($*p < 0.05$, $**p < 0.01$). Error bars represent standard deviations from the mean ($n = 3$).

3.3. *In vitro* release kinetics of P28 and degradation characterization

As shown in Fig. 4a, the cumulative release amount of P28 from different scaffolds was measured. P28 was quickly released from the ECM matrix, while the matrix maintained a high retention rate of P28/PlGF-$2_{123\text{-}144*}$ in the SIS/PLA/P28/PlGF-$2_{123\text{-}144*}$ group. At the initial phase, the release rates were very high. On the first day, the release rates of P28 from SIS/PLA/P28 and SIS/PLA/P28/PlGF-$2_{123\text{-}144*}$ were 31.33 + 4.44% and 22.19 + 2.88%, respectively. The release rates began to decrease on the second day and then gradually stabilized; the cumulative release rates were 77.10 + 4.26% and 36.59 + 3.57%, respectively, over 21 days. We also measured the enzymatic release of P28 from the SIS/PLA/P28/PlGF-$2_{123\text{-}144*}$ scaffold. We hypothesized that PlGF-$2_{123\text{-}144*}$-fused P28 could be released from the scaffold by the degeneration of the ECM matrix due to its high affinity to PlGF-$2_{123\text{-}144*}$. Collagenase type I was chosen to perform the enzymatic release experiment due to its enzymolysis ability of collagen fiber in SIS/PLA. With the aid of collagenase, the release rate of P28 in the scaffolds was found to instantly increase and then plateau in the first 3 days. The SIS/PLA scaffold lost 82.92 + 6.69% of its total weight after 3 days during the degradation process (Fig. 4b). Generally, the release rate of P28 was accordance with the weight loss rate for collagenase due to an enzymatic mechanism. As the heparin-binding domain of PlGF-2 was cleaved by plasmin, P28/PlGF-$2_{123\text{-}144*}$ was embedded onto SIS/PLA, which was incubated in biological buffer without or with plasmin. With plasmin, P28 experienced a burst-like release from SIS/PLA. By contrast, a slower and more sustained release of P28 was observed in the absence of plasmin.

3.4. Cell viability and proliferation

Live cells stained with calcein-AM (green) were measured after seeding the BMSCs seeded onto the scaffolds for 7 days (Fig. 5a). The total number (TN) of SIS/PLA/P28 and SIS/PLA/P28/PlGF-$2_{123\text{-}144*}$ scaffolds were 34.72 ± 3.18 and 50.4 ± 2.61

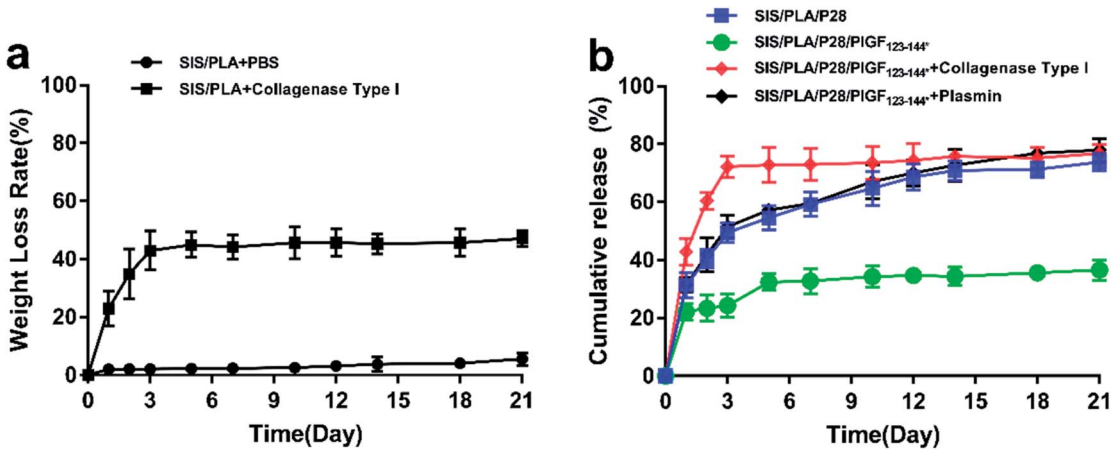

Fig. 4 (a) The weight loss rate of SIS/PLA with or without 4 mg mL^{-1} of collagenase type I during incubation. (b) *In vitro* enzymatic release of P28 from the SIS/PLA scaffolds. Error bars represent standard deviations from the mean ($n = 3$).

per square millimeter, respectively. This was significantly greater than that of the SIS/PLA and SIS/PLA/PlGF-$2_{123\text{-}144*}$ scaffolds (23.29 ± 2.66 and 23.64 ± 1.31 per square millimeter, respectively) (Fig. 5b).

Cell proliferation on the different types of scaffold was detected using the MTT assay after incubation for 1, 3, 5, and 7 days. The numbers of BMSCs continued to increase from the first to the 7th day. The number of BMSCs in the SIS/PLA/P28 and SIS/PLA/P28/PlGF-$2_{123\text{-}144*}$ groups were significantly higher than those in the SIS/PLA and SIS/PLA/PlGF-$2_{123\text{-}144*}$ groups. The proliferation rate of BMSCs was significantly higher on SIS/PLA/P28/PlGF-$2_{123\text{-}144*}$ compared to SIS/PLA/P28 (Fig. 5c).

3.5. Osteogenic differentiation of BMSCs

The ALP activity is used as an initial marker of osteogenic differentiation. From the 5th to 15th day, the ALP activity of each group increased sustainably. The ALP activity in the SIS/PLA/P28 and SIS/PLA/P28/PlGF-$2_{123\text{-}144*}$ groups significantly increased compared with that of the SIS/PLA and SIS/PLA/PlGF-

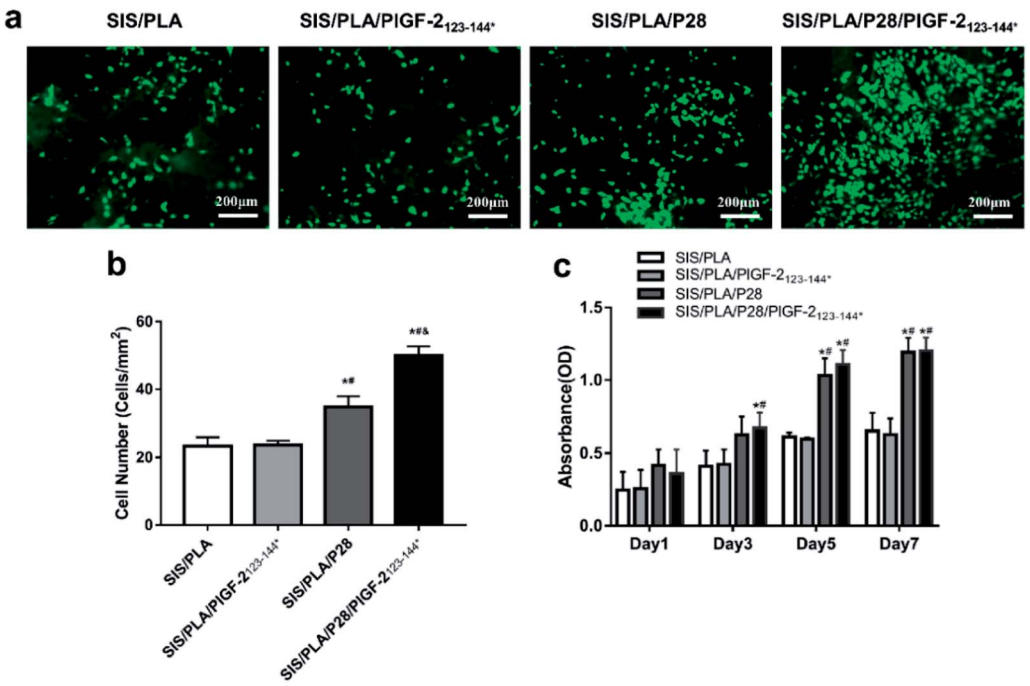

Fig. 5 Viability of BMSCs within SIS/PLA, SIS/PLA/PlGF-$2_{123\text{-}144*}$, SIS/PLA/P28, and SIS/PLA/P28/PlGF-$2_{123\text{-}144*}$ scaffolds. (a) Representative fluorescence images of cells on membranes at day 7. (b) Total adhesive cell numbers of BMSCs in SIS/PLA, SIS/PLA/PlGF-$2_{123\text{-}144*}$, SIS/PLA/P28, and SIS/PLA/P28/PlGF-$2_{123\text{-}144*}$ groups. (c) BMSCs proliferation in SIS/PLA, SIS/PLA/PlGF-$2_{123\text{-}144*}$, SIS/PLA/P28, and SIS/PLA/P28/PlGF-$2_{123\text{-}144*}$ groups. Statistical significance is indicated by $^{*}p < 0.05$ compared with the SIS/PLA group, $^{\#}p < 0.05$ compared with the SIS/PLA/PlGF-$2_{123\text{-}144*}$ group, and $^{\&}p < 0.05$ compared with the SIS/PLA/P28 group. Error bars represent standard deviations from the mean ($n = 3$).

$2_{123\text{-}144*}$ groups, and no significant difference existed between the groups with P28 and with P28/PlGF-$2_{123\text{-}144*}$ (Fig. 6a).

Western blotting (Fig. 6b) was used to analyze the intracellular expression of osteogenesis-related markers, Col-Iα, osteopontin (OPN), osteocalcin (OCN), and Runx2, as well as BMP signaling-related Smad1/5/8 and phosphorylated Smad1/5/8. The expression levels of Col-Iα, Runx2, OPN, and OCN were significantly increased in the SIS/PLA/P28 and SIS/PLA/P28/PlGF-$2_{123\text{-}144*}$ groups at 14 days compared with those in the pure SIS/PLA scaffold. Notably, the protein levels of OPN and OCN expression were significantly increased in the BMSCs on SIS/PLA/P28/PlGF-$2_{123\text{-}144*}$ scaffold compared to those in the SIS/PLA/P28 scaffold, possibly owing to the fact that the rapid release of P28 leads to the overexpression of later markers of osteogenic differentiation. Next, we assessed whether P28 and P28/PlGF-$2_{123\text{-}144*}$ effectively activated BMP-2-Smad1/5/8 signaling. For phospho-Smad1/5/8 expression, the SIS/PLA/PlGF-$2_{123\text{-}144*}$ and SIS/PLA/P28/PlGF-$2_{123\text{-}144*}$ groups showed an increase compared with the SIS/PLA and SIS/PLA/PlGF-$2_{123\text{-}144*}$ groups.

The expression of osteogenesis-related genes was measured by RT-PCR (Fig. 6c). In accordance with the blotting results, the expression levels of Runx2, Col-Iα, OCN, OPN, and BMP2 were both significantly increased in the SIS/PLA/P28 and SIS/PLA/P28/PlGF-$2_{123\text{-}144*}$ groups at 14 days compared with those in pure SIS/PLA and SIS/PLA/PlGF-$2_{123\text{-}144*}$ groups ($p < 0.05$). The expression levels of OCN increased by approximately 40-fold in SIS/PLA, shown to be most responsive to P28 among all genes.

3.6. General conditions of animals

All animals were awake 1 h post-surgery, and their incisions healed by the second week after surgery. All animals began to eat in the first day and their limbs were not weight bearing at 1 week after surgery; the limbs could bear sufficient weight to

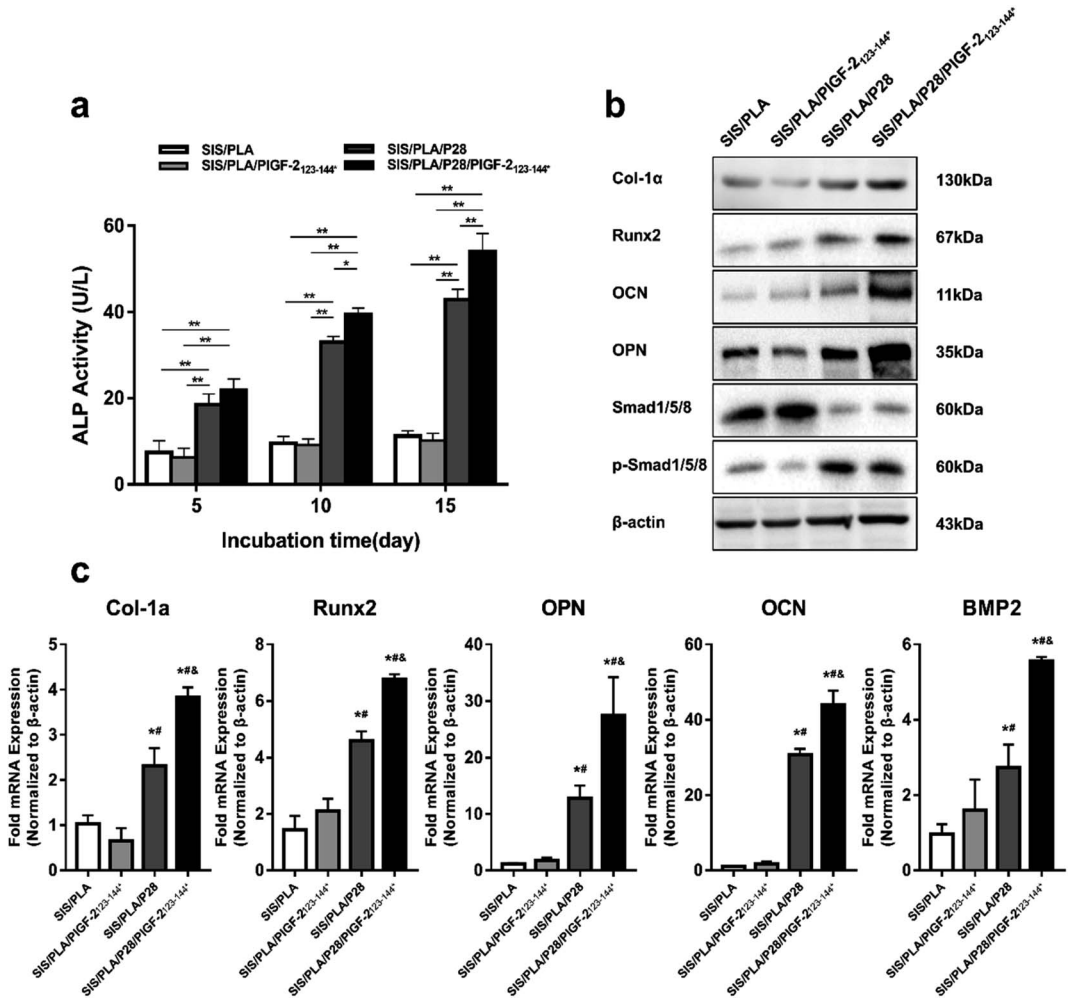

Fig. 6 Assays of osteogenic differentiation of BMSCs. (a) Alkaline phosphatase (ALP) activity in SIS/PLA, SIS/PLA/PlGF-$2_{123\text{-}144*}$, SIS/PLA/P28, and SIS/PLA/P28/PlGF-$2_{123\text{-}144*}$ groups (*$p < 0.05$, **$p < 0.01$). (b) Western blotting analysis of Col-1α, Runx2, OCN, OPN, and Smad1/3/5 proteins in BMSCs on the different scaffolds at 14 days. (c) Gene expression profile of osteogenic differentiation-related gene and BMP-2 of BMSCs cultured on different scaffolds for 14 days. Statistical significance is indicated by *$p < 0.05$ compared with the SIS/PLA group, $^{\#}p < 0.05$ compared with the SIS/PLA/PlGF-$2_{123\text{-}144*}$ group, and $^{\&}p < 0.05$ compared with the SIS/PLA/P28 group. Error bars represent standard deviations from the mean ($n = 3$).

walk at 4 weeks after surgery, and at 8 weeks, the animals had returned to normal activities. The wounds in the implant areas of the animals healed well without any infection. No canine was excluded from the analysis. The animal surgical procedures are shown in Fig. 7.

3.7. Radiographic examination

As shown in Fig. 8a, the control group showed no new bone formation in the bone defect region at 12 and 24 weeks, and over time, the broken ends of the radials assimilated and atrophied. The SIS/PLA group showed no new bone formation and callus in the defect region at 12 weeks, and there were only small amounts of new bone in the defect regions generated at both ends at 24 weeks.

At 12 weeks, the defect region had become blurred and fuzzy callus formation was observed in the SIS/PLA/P28 and SIS/PLA/P28/PlGF-$2_{123\text{-}144*}$ groups; at 24 weeks the SIS/PLA/P28 group showed that the defect region had been almost completely replaced with high density shadows and showed more callus shadow. In addition, the scaffolds in all the groups showed certain degradation. The Lane–Sandhu X-ray scores in the SIS/PLA/P28 and SIS/PLA/P28/PlGF-$2_{123\text{-}144*}$ groups were markedly higher than in the SIS/PLA and SIS/PLA/PlGF-$2_{123\text{-}144*}$ groups at 24 weeks in postoperative canines (Fig. 8c).

3.8. 3D-CT evaluation

At 12 and 24 weeks after surgery, 3D-CT images (Fig. 8b) were obtained to assess the new bone formation of the radial bone defects, characterized by bone tissue coverage of the defects. As shown in Fig. 8b_1, b_3, b_5 and b_7 for 12 weeks post-operation, the SIS/PLA and SIS/PLA/PlGF-$2_{123\text{-}144*}$ groups showed little new bone formation, and the defect region had not been barely repaired. On the contrary, loading with P28 and P28/PlGF-$2_{123\text{-}144*}$ led to a marked increase in bone tissue coverage in the other two groups, yielding a coverage at 78.88 ± 6.26% in the SIS/PLA/P28/PlGF-$2_{123\text{-}144*}$ group and 61.80 ± 11.10% in the SIS/PLA/PlGF-$2_{123\text{-}144*}$ group. At 24 weeks post-operation, the implant zone was wrapped with new bone tissue in the SIS/PLA/P28 group, while the SIS/PLA/P28/PlGF-$2_{123\text{-}144*}$ group showed a defect area that had been mostly filled with new bone tissue, with only a small aperture remaining (Fig. 8b_6 and b_8). A graft of SIS/PLA within P28/PlGF-$2_{123\text{-}144*}$ mildly increased the bone tissue coverage when compared to the healing of defects of pure P28, yielding a coverage of 93.87 ± 4.00% in the SIS/PLA/P28/PlGF-$2_{123\text{-}144*}$ group and 77.22 ± 8.40% in the SIS/PLA/PlGF-$2_{123\text{-}144*}$ group (Fig. 8d). On the other hand, in the SIS/PLA and SIS/PLA/PlGF-$2_{123\text{-}144*}$ groups, only some new bone formation was visible at both ends of the defect, and the defect had not been fully restored (Fig. 8b_2 and b_4).

3.9. Histological examination

We then evaluated the new peri-implant bone formation by histological analysis of the longitudinal sections (parallel to the long axis of radius). HE staining and Masson staining was conducted as shown in Fig. 9a. No distinct adverse inflammatory reaction was observed at 12 weeks and 24 weeks. In every group, the pores of the residual materials were filled with fibrous connective tissue at 12 weeks. The defects in the SIS/PLA and SIS/PLA/PlGF-$2_{123\text{-}144*}$ groups did not show any new bone tissue; nevertheless, the defects transplanted with SIS/PLA/P28 and SIS/PLA/P28/PlGF-$2_{123\text{-}144*}$ group showed small amounts of new bone scattered across the full length of the implant. At 24 weeks, the material pores of SIS/PLA were found to be completely degraded. The material pores of each group were filled with large amounts of new bone and cartilage tissue connected in pieces, and numerous active osteoblasts were attached to the new bone tissue. In addition, the cartilage tissue showed a tendency to transform into mature bone tissue, with no boundaries observed between the materials. The bone defect margins could be observed, indicating that the materials had been completely degraded. The area of trabecular in the SIS/PLA/P28 and SIS/PLA/P28/PlGF-$2_{123\text{-}144*}$ groups evidently exceeded that of the other two groups. The measured areas of the new bone in each group are shown in Fig. 9a. The amount of new bone increased from 12 to 24 weeks in all groups. The SIS/PLA/P28 and SIS/PLA/P28/PlGF-$2_{123\text{-}144*}$ groups showed statistically significant differences with the SIS/PLA and SIS/PLA/P28/PlGF-$2_{123\text{-}144*}$ groups ($p < 0.01$), while the SIS/PLA/P28 group was significantly different from the SIS/PLA/P28/PlGF-$2_{123\text{-}144*}$ group at 24 weeks ($p < 0.05$).

We subsequently examined the expression profiles for OCN associated with osteogenic differentiation by IHC staining at 24 weeks. OCN-positive staining was weak in the SIS/PLA and SIS/PLA/PlGF-$2_{123\text{-}144*}$ groups, but became apparent in the SIS/PLA/P28 group. OCN-positive staining was strongest in the SIS/PLA/P28/PlGF-$2_{123\text{-}144*}$ group. There was no significant difference in the expression of OCN between the SIS/PLA/PlGF-$2_{123\text{-}144*}$ and SIS/PLA groups. This result confirmed that the P28-loaded SIS/PLA availably increased the expression of OCN and facilitated osteogenic differentiation (Fig. 9b and c).

4. Discussion

Allografts have showed a high failure rate and substantial limitations in their integration with host bone, due to infection,

Fig. 7 Animal surgical procedures: (a) macroscopic view of the SIS/PLA scaffold materials; (b) macroscopic appearance of a radial bone defect; (c) material implanted into the defect region; (d) the defect region was fixed with a steel plate; (e) appearance of the surgical site post-operation.

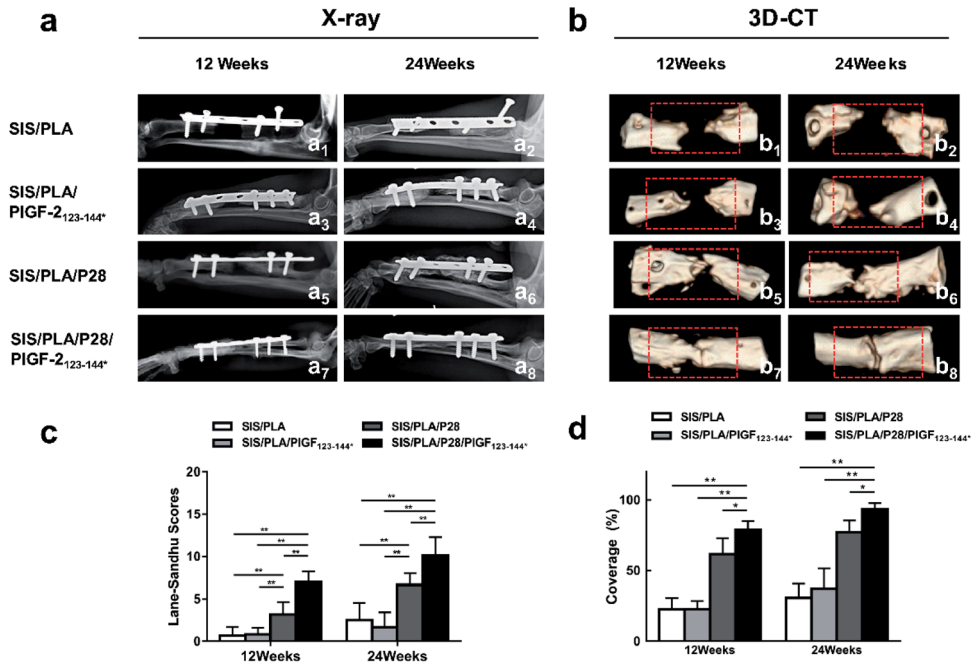

Fig. 8 (a) Radiographs of the implants in the four groups at 12 and 24 weeks after surgery. (b) 3D-CT scan photos of the radial bone defect sites in the four groups at 12 and 24 weeks after surgery. (c) Lane–Sandhu X-ray scores of five groups at 12 and 24 weeks. (d) Quantification of the percentage area of newly formed bone for the different materials at 12 and 24 weeks after surgery (*$p < 0.05$, **$p < 0.01$). Error bars represent standard deviations from the mean ($n = 6$).

fracture, and non-union, in 5 and 10 year clinical follow-up studies on massive bone defects. In this context, functionalized artificial bone materials that deliver bone growth factors with temporal precision have proven to be an effective strategy for repairing massive bone defects. In this study, we sought to design a biomimetic material coated with degradable polymer that would act as a vehicle for osteogenic factors. In a previous study, Dewey *et al.* reported that a collagen–PLA composite promotes osteogenic differentiation of porcine adipose stem cells.[35] In our previous study, we manufactured SIS-mesoporous bioactive glass (MBG) composite materials that exhibited high osteogenic and angiogenic capacity.[16] Therefore, we believe that

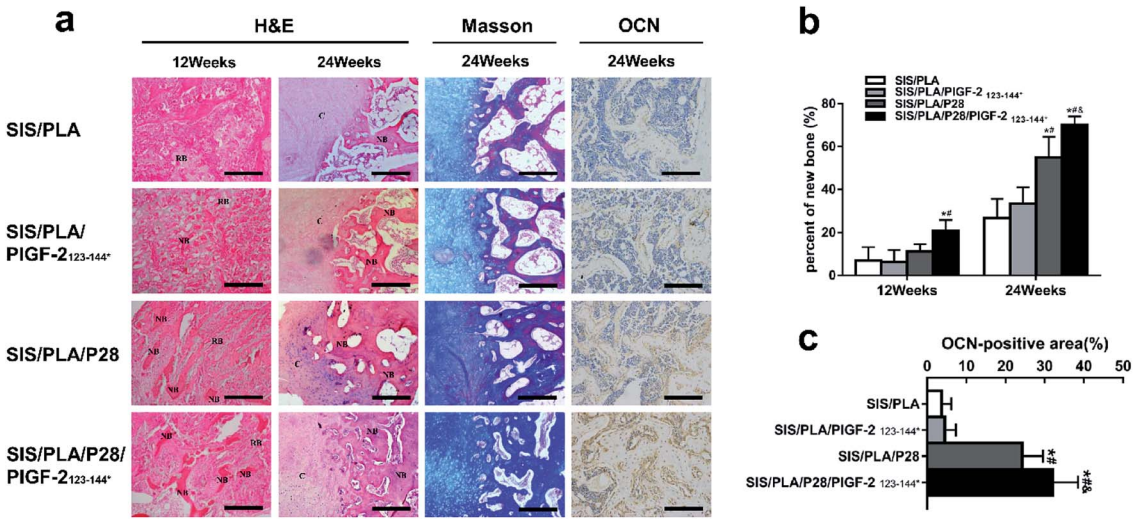

Fig. 9 (a) H&E and Masson stained sections of the different groups in the region of the bone defect at 12 and 24 weeks after surgery. "NB" represents the new bone; "RB" represents the remaining biomaterials; "C" represents cartilage tissue (original magnification: ×100); immunohistochemical staining for OCN at 24 weeks after implantation (original magnification: ×100). (b) New bone area ratio determined by histomorphometric analysis. (c) OCN-positive area determined by histomorphometric analysis. Statistical significance is indicated by *$p < 0.05$ compared with SIS/PLA group, $^{\#}p < 0.05$ compared with the SIS/PLA/PlGF-$2_{123\text{-}144*}$ group, and $^{\S}p < 0.05$ compared with the SIS/PLA/P28 group.

the recombination of biodegradable polymers and natural extracellular matrix materials can be extremely useful in the fabrication of new generation artificial bone materials.

SIS/PLA was designed based on the principle of biomimetics, with both composition and structure being similar to natural bone. Its pore size of 100–300 μm may provide a superior structure:[25] macropores with a pore diameter in the range of 50–300 μm are required for cell penetration and neovascularization with a scaffold *in vivo*. Previous studies have demonstrated the outstanding biocompatibility and non-immunogenicity of SIS.[16,24] The addition of PLA is expected to improve the mechanical properties of SIS and allow for the tuning of its degradation time. Previous studies have also mixed biodegradable polymers with natural polymer materials.[16,36]

BMP-2 related peptides represent an effective method to improve the disadvantages associated with the clinical treatment of bone defects using BMP-2. The ability to combine a small peptide with various scaffold materials can be further enhanced through the modification of the structure with small molecule peptides, which both increases the amount of peptide drug retained on the scaffolds and reduces the release rate. In the current study, the peptide P28, which contains repetitive acidic amino acids in its molecular structure, was utilized to achieve a small relative molecular weight, as well as a better stability and linear structure. These traits may facilitate the execution of its biological effect and promote favorable function without producing unfavorable side effects. In addition, the active site of short-chain polypeptides can be completely exposed between the cell membrane receptors to obtain higher bioactivity. Enhanced efficacy may also be facilitated by the repetitive acidic amino acids and phosphorylated serine, due to their high affinity to hydroxyapatite and calcium phosphate, respectively.[37–39]

Physiologically, the interactions between osteogenic factors and the components of the extracellular matrix (ECM) facilitate the differentiation of *in situ* stem/progenitor cells into osteoblasts by local and spatial regulation of signaling. However, the supra-physiological release of osteogenic factors due to the lack of ECM binding could underlie the limited translation of these materials to clinical applications. Matrices grafted with PlGF-$2_{123\text{-}144*}$ fused BMP2 have been demonstrated to enhance the sustained release of BMP2 protein and promote the regeneration of intramembranous ossification compared with fibrin loaded with BMP2 only.[27] As shown in Fig. 3, we designed a PlGF-$2_{123\text{-}144*}$-functionalized material to reinforce the efficacy of P28 immobilization on SIS/PLA and facilitate its temporal and precise release. *In vitro*, the study of enzymatic release kinetics demonstrated that for the SIS/PLA scaffolds, the majority of the P28 peptide was localized superficially with weak bonds, causing an initial burst release during the first three days. Subsequently, the release rates of P28 began to slow; however, the proportion of P28 released was clearly more than that of PlGF-$2_{123\text{-}144*}$-fused P28. Moreover, the retention of PlGF-$2_{123\text{-}144*}$-fused P28 in SIS/PLA reduced with the cleavage of PlGF-$2_{123\text{-}144*}$ by plasmin. Thus, it appeared that PlGF-$2_{123\text{-}144*}$-fused P28 combined with the scaffolds in a stronger manner than P28, contributing to the high affinity of PlGF-$2_{123\text{-}144*}$ to ECM protein. In addition, P28 was rapidly released from scaffold in a burst, and reached to a plateau within the first 3 days, which is accordance with the weight loss rate of scaffolds in the presence of collagenase, as shown in Fig. 4a. This suggests that the enhanced material retention and lower P28 concentration in bone tissue may improve the potency of P28 in exerting osteogenic bioactivity used in our previous study.[25]

We then focused on verifying the biological activity of P28 and PlGF-$2_{123\text{-}144*}$ fused P28 in subsequent cell and animal experiments. The effects of the scaffold material on cell behavior are a result of the interactions between the ligand on the scaffold surface and the receptors on the cells.[39] The slow release of growth factors on the scaffold may therefore produce a long-term effect on cell migration, adhesion, proliferation, and differentiation.[40] *In vitro*, the BMSCs were implanted in four groups of materials, and the subsequent adhesion, proliferation, and differentiation were observed. The results showed that the adhesion, proliferation, and ALP levels of the groups combined with P28 or P28/PlGF-$2_{123\text{-}144*}$ were superior to those of the scaffold groups without P28 or P28/PlGF-$2_{123\text{-}144*}$. This difference was found to increase significantly over time. Furthermore, the expression of phospho-Smad1/5/8 protein and BMP-2 gene enhanced in the SIS/PLA/P28 and SIS/PLA/P28/PlGF-$2_{123\text{-}144*}$ groups as P28 showed BMP-2-like activation of the BMP-2-Smad1/3/5 pathway at 7 days.

The repair of the bone defects, particularly the repair of critical-size bone defects that do not spontaneously and naturally heal, is the ultimate goal of bone tissue engineering research.[41] For long bones, critical-size bone defects represent defects with a length that is 1.5–2 times longer than the bone diameter. In our *in vivo* study, a 20 mm segmental defect was created in the radial bone. At 12 and 24 weeks after surgery, the defects in the blank group, which had no material implanted in the defect, were poorly repaired and exhibited marginal new bone tissue formation. Thus, we consider that the critical-size bone defects in this study were accurate and credible. At 24 weeks after surgery, X-ray and 3D-CT analysis showed that the implanted materials of the SIS/PLA/P28 and SIS/PLA/P28/PlGF-$2_{123\text{-}144*}$ groups fused naturally with the host bone. The bone defects appeared to have been completely repaired (Fig. 8). Histological examination revealed a large amount of new bone tissue formation, and demonstrated that the interspace of the biomaterials was almost fully replaced by new bone with a clear resorption of the materials. Histomorphometry indicated that the new bone formation of the P28 or P28/PlGF-$2_{123\text{-}144*}$ groups were significantly higher than those without P28. Furthermore, the expression of OCN associated with osteogenic differentiation on SIS/PLA/P28/PlGF-$2_{123\text{-}144*}$ showed the strongest positive IHC staining, which represents a slight inconformity with the *in vitro* results. This difference could be due to the long-term observation time window *in vivo*, which will help us to confirm the sustained delivery of growth factor strengthen the osteogenic capability *in vivo*. Although the defects that had been implanted with SIS/PLA materials were not repaired, the defect area was reduced to some degree because the new bone formation had occurred in the ends of the defect. These results suggested that the incorporation of P28/PlGF-$2_{123\text{-}144*}$ may

accelerate the formation of new bone tissue sufficiently to overcome the degradation of scaffold materials.

5. Conclusions

In summary, in this study, we generated a type of engineered P28 variants with super-affinity to biomimetic SIS/PLA allografts. This high-affinity P28 material was demonstrated to retain and deliver P28 peptide. It was demonstrated that the P28 peptide was also able to exhibit a long-term release from PlGF-$2_{123\text{-}144*}$-functionalized SIS/PLA artificial material. This material displayed cell adhesion, proliferation, and differentiation properties *in vitro* and repaired massive bone defects *in vivo*, exceeding the rate of repair using pure P28 alone. This resulted in a clear reduction in the dose of P28 needed for bone regeneration. Together, this novel approach for the healing of massive bone defects using a temporal pattern system of controlled release growth factor has promising clinical application prospects in bone tissue engineering.

Conflicts of interest

The authors declare no competing financial interests.

Acknowledgements

This research was supported by grants from the National Natural Science Foundation of China (grant numbers 81672158 and 81873999), Youth Program of National Natural Science Foundation of China (grant number 81902219), and the National Key R&D Program of China (2016YFC1100100).

References

1 Y. M. Kolambkar, J. D. Boerckel, K. M. Dupont, M. Bajin, N. Huebsch, D. J. Mooney, D. W. Hutmacher and R. E. Guldberg, *Bone*, 2011, **49**, 485–492.
2 S. Koehler, F. Raslan, C. Stetter, S. M. Rueckriegel, R. I. Ernestus and T. Westermaier, *J. Neurosurg. Spine*, 2016, **24**, 309–314.
3 D. S. Garbuz, B. A. Masri and A. A. Czitrom, *Orthop. Clin. N. Am.*, 1998, **29**, 199–204.
4 A. M. Jakoi, J. A. Iorio and P. J. Cahill, *Musculoskelet Surg.*, 2015, **99**, 171–178.
5 R. S. Neto, A. Stavropoulos, F. L. Coletti, R. S. Faeda, L. Pereira and E. Marcantonio, *Clin. Oral Implants Res.*, 2014, **25**, 226–233.
6 R. Soni, N. V. Kumar, S. Chameettachal, F. Pati and S. N. Rath, *Mater. Today: Proc.*, 2019, **15**, 294–299.
7 N. Bakhshalian, H. Nowzari, K.-M. Ahn and B. H. Arjmandi, *J. West Soc. Periodontol. Periodontal. Abstr.*, 2014, **62**, 35–38.
8 K. M. Scheufler and D. Diesing, *Orthopade*, 2015, **44**, 146–153.
9 S. Gitelis and B. J. Cole, *Instr. Course Lect.*, 2002, **51**, 507–520.
10 R. Y. Basha, T. S. S. Kumar and M. Doble, *Mater. Sci. Eng., C*, 2015, **57**, 452–463.
11 S. Sankar, M. Kakunuri, S. D. Eswaramoorthy, C. S. Sharma and S. N. Rath, *J. Tissue Eng. Regener. Med.*, 2018, **12**, E2073–E2084.
12 A. K. Mahanta, D. K. Patel and P. Maiti, *ACS Biomater. Sci. Eng.*, 2019, **5**, 5139–5149.
13 S. R. K. Meka, V. Agarwal and K. Chatterjee, *Mater. Sci. Eng., C*, 2019, **94**, 565–579.
14 S. R. K. Meka, S. K. Verma, V. Agarwal and K. Chatterjee, *ChemistrySelect*, 2018, **3**, 3762–3773.
15 L. T. Saldin, M. C. Cramer, S. S. Velankar, L. J. White and S. F. Badylak, *Acta Biomater.*, 2017, **49**, 1–15.
16 T. F. Sun, M. Liu, S. Yao, Y. H. Ji, Z. K. Xiong, K. Tang, K. F. Chen, H. Yang and X. D. Guo, *Tissue Eng., Part A*, 2018, **24**, 1044–1056.
17 S. L. VoytikHarbin, A. O. Brightman, M. R. Kraine, B. Waisner and S. F. Badylak, *J. Cell. Biochem.*, 1997, **67**, 478–491.
18 C. S. Kim, J. I. Kim, J. Kim, S. H. Choi, J. K. Chai, C. K. Kim and K. S. Cho, *Biomaterials*, 2005, **26**, 2501–2507.
19 S. D. Boden, J. Kang, H. Sandhu and J. G. Heller, *Spine*, 2002, **27**, 2662–2673.
20 J. R. Dimar, S. D. Glassman, J. K. Burkus, P. W. Pryor, J. W. Hardacker and L. Y. Carreon, *J. Bone Jt. Surg., Am. Vol.*, 2009, **91**, 1377–1386.
21 J. R. Dimar, S. D. Glassman, K. J. Burkus and L. Y. Carreon, *Spine*, 2006, **31**, 2534–2539.
22 M. Boakye, P. V. Mummaneni, M. Garrett, G. Rodts and R. Haid, *J. Neurosurg. Spine*, 2005, **2**, 521–525.
23 J. K. Burkus, M. F. Gornet, T. C. Schuler, T. J. Kleeman and T. A. Zdeblick, *J. Bone Jt. Surg., Am. Vol.*, 2010, **92**, 2615–2616.
24 T. F. Sun, M. Liu, S. Yao, Y. H. Ji, L. Shi, K. Tang, Z. K. Xiong, F. Yang, K. F. Chen and X. D. Guo, *Int. J. Nanomed.*, 2018, **13**, 791–804.
25 T. F. Sun, Y. Z. Qu, W. Cui, L. Yang, Y. H. Ji, W. Yu, R. Navinduth, Z. W. Shao, H. Yang and X. D. Guo, *J. Biomed. Mater. Res., Part A*, 2018, **106**, 210–220.
26 W. Cui, Q. Q. Liu, L. Yang, K. Wane, T. F. Sun, Y. H. Ji, L. P. Liu, W. Yu, Y. Z. Qu, J. W. Wang, Z. G. Zhao, J. T. Zhu and X. D. Guo, *ACS Biomater. Sci. Eng.*, 2018, **4**, 211–221.
27 M. M. Martino, P. S. Briquez, E. Guc, F. Tortelli, W. W. Kilarski, S. Metzger, J. J. Rice, G. A. Kuhn, R. Muller, M. A. Swartz and J. A. Hubbell, *Science*, 2014, **343**, 885–888.
28 E. Aydin, J. A. Planell and V. Hasirci, *J. Mater. Sci.: Mater. Med.*, 2011, **22**, 2413–2427.
29 J. C. Luo, W. Chen, X. H. Chen, T. W. Qin, Y. C. Huang, H. Q. Xie, X. Q. Li, Z. Y. Qian and Z. M. Yang, *Biomaterials*, 2011, **32**, 706–713.
30 C. Wu, Y. Zhang, Y. Zhu, T. Friis and Y. Xiao, *Biomaterials*, 2010, **31**, 3429–3438.
31 R. C. Thomson, M. J. Yaszemski, J. M. Powers and A. G. Mikos, *Biomaterials*, 1998, **19**, 1935–1943.
32 B. K. Culpepper, W. M. Webb, P. P. Bonvallet and S. L. Bellis, *J. Biomed. Mater. Res., Part A*, 2014, **102**, 1008–1016.
33 J. F. Li, Q. X. Zheng, X. D. Guo, Z. W. Zou, Y. D. Liu, S. H. Lan, L. B. Chen and Y. Deng, *Biomed. Mater.*, 2013, **8**, 10.

34 L. Yang, J. H. Huang, S. Y. Yang, W. Cui, J. P. Wang, Y. P. Zhang, J. F. Li and X. D. Guo, *ACS Biomater. Sci. Eng.*, 2018, **4**, 3246–3258.
35 M. J. Dewey, E. M. Johnson, D. W. Weisgerber, M. B. Wheeler and B. A. C. Harley, *J. Mech. Behav. Biomed. Mater.*, 2019, **95**, 21–33.
36 M. Parmaksiz, A. E. Elcin and Y. M. Elcin, *Mater. Sci. Eng., C*, 2019, **94**, 788–797.
37 J. Y. Lee, J. E. Choo, H. J. Park, J. B. Park, S. C. Lee, S. J. Lee, Y. J. Park and C. P. Chung, *J. Biomed. Mater. Res., Part A*, 2008, **87A**, 688–697.
38 S. Kasugai, R. Fujisawa, Y. Waki, K. Miyamoto and K. Ohya, *J. Bone Miner. Res.*, 2000, **15**, 936–943.
39 A. Gericke, C. Qin, L. Spevak, Y. Fujimoto, W. T. Butler, E. S. Sorensen and A. L. Boskey, *Calcif. Tissue Int.*, 2005, **77**, 45–54.
40 M. Farokhi, F. Mottaghitalab, M. A. Shokrgozar, K. L. Ou, C. B. Mao and H. Hosseinkhani, *J. Controlled Release*, 2016, **225**, 152–169.
41 E. Quinlan, E. M. Thompson, A. Matsiko, F. J. O'Brien and A. Loez-Noriega, *J. Controlled Release*, 2015, **207**, 112–119.

